JACS
JOURNAL OF THE AMERICAN CHEMICAL SOCIETY
Communication
pubs.acs.org/JACS

A New Core/Shell NiAu/Au Nanoparticle Catalyst with Pt-like Activity for Hydrogen Evolution Reaction

Haifeng Lv,[†,‡,∥] Zheng Xi,[†,∥] Zhengzheng Chen,[§] Shaojun Guo,[†] Yongsheng Yu,[⊥] Wenlei Zhu,[†] Qing Li,[†] Xu Zhang,[§] Mu Pan,[‡] Gang Lu,*[,§] Shichun Mu,*[,‡] and Shouheng Sun*[,†]

[†]Department of Chemistry, Brown University, Providence, Rhode Island 02912, United States
[‡]State Key Laboratory of Advanced Technology for Materials Synthesis and Processing, Wuhan University of Technology, Wuhan, 430070, China
[§]Department of Physics and Astronomy, California State University Northridge, Northridge, California 91330, United States
[⊥]School of Chemical Engineering and Technology, Harbin Institute of Technology, Harbin, Heilongjiang 150001, China

Supporting Information

ABSTRACT: We report a general approach to NiAu alloy nanoparticles (NPs) by co-reduction of $Ni(acac)_2$ (acac = acetylacetonate) and $HAuCl_4{\cdot}3H_2O$ at 220 °C in the presence of oleylamine and oleic acid. Subject to potential cycling between 0.6 and 1.0 V (vs reversible hydrogen electrode) in 0.5 M H_2SO_4, the NiAu NPs are transformed into core/shell NiAu/Au NPs that show much enhanced catalysis for hydrogen evolution reaction (HER) with Pt-like activity and much robust durability. The first-principles calculations suggest that the high activity arises from the formation of Au sites with low coordination numbers around the shell. Our synthesis is not limited to NiAu but can be extended to FeAu and CoAu as well, providing a general approach to MAu/Au NPs as a class of new catalyst superior to Pt for water splitting and hydrogen generation.

Hydrogen evolution reaction (HER) is often referred to as electrochemical reduction of protons to hydrogen (H_2) and is an important half reaction used to couple with oxygen evolution reaction in water splitting. It has been studied extensively as a sustainable way of producing H_2 for clean energy applications.[1] For HER to proceed smoothly without consuming extra energy, a catalyst must be present to initiate proton reduction with minimal overpotential.[2] Past studies have identified Pt-based catalysts as being the most effective in catalyzing HER due to their low reduction overpotentials and fast reduction kinetics in acidic media.[3] To overcome the cost issues related to the Pt catalysts, recent efforts have been devoted to developing new catalysts from earth-abundant elements, such as Mo, W, and Ni and their molecular derivatives.[4] Despite the promising catalysis demonstrated on HER, these catalysts are generally much inferior to the Pt-based ones with relatively high overpotentials. Consequently a new class of non-Pt catalysts with their catalysis superior to or comparable with Pt catalysts is still desperately needed before water splitting can be applied practically for hydrogen generation.

Here we report a new catalyst based on core/shell NiAu/Au nanoparticles (NPs) for highly efficient HER. Nanoscale Au has been studied extensively as catalyst for chemical reactions, including CO oxidation,[5] O_2 reduction,[6] and CO_2 reduction.[7] Especially, Au catalyst obtained from electro-anodization of Au shows much enhanced catalysis for electrochemical reduction of CO_2 to CO,[7b] and Au NPs with Au on the corner sites are more active for HER than for electrochemical reduction of CO_2 in $KHCO_3$ solution.[7c] These observations on Au catalysis, combining with recent studies on tuning electrocatalysis of the core/shell structures for electrochemical reduction reactions, motivated us to study core/shell M/Au NPs as a non-Pt catalyst for HER with M being a first-row transition metal. We first tested the direct synthesis of Ni/Au core/shell NPs without much success. However, when we prepared and studied NiAu alloy NPs, we found that these alloy NPs behaved similarly to CuPt or FePt NPs on electro-anodization,[8] and their surface Ni could be etched in a more controlled manner by electro-anodization in an acid solution, giving core/shell NiAu/Au NPs. These core/shell NPs were more active for HER in an acid solution than either NiAu or Au NPs. They were nearly as active as the commercial Pt catalyst but with much enhanced durability.

To prepare NiAu alloy NPs, we developed a new method of co-reducing $Ni(acac)_2$ (acac = acetylacetonate) and $HAuCl_4{\cdot}3H_2O$ with oleylamine (OAm) at 220 °C. Due to the large Ni/Au miscibility gap and reduction potential difference, NiAu NPs are not easily made and previous methods often lead to polydisperse NiAu NPs or mixture of Au and Ni NPs.[9] Recently, we found that $M(acac)_2$ and $Pt(acac)_2$ with different reduction potentials could be readily co-reduced by a weak organic reducing agent, such as OAm, to form MPt NPs with M being Fe, Co, Ni, etc.[10] We extended this synthesis and succeeded in preparing monodisperse NiAu NPs with size and composition controls. In the synthesis, we simply reacted $Ni(acac)_2$ and $HAuCl_4{\cdot}3H_2O$ with OAm in the presence of small amount of oleic acid (OA) at 220 °C. Here, OAm served as the solvent, surfactant, and reducing agent, while OAm and OA functioned as alloy NP stabilizers. By reacting 0.2 mmol of $HAuCl_4{\cdot}3H_2O$ with 0.25 mmol of $Ni(acac)_2$, we obtained $Ni_{43}Au_{57}$ NPs as measured by inductively coupled plasma-atomic emission spectroscopy (ICP-AES). In the synthesis, Ni/Au compositions were controlled by the molar ratio of $Ni(acac)_2$ and $HAuCl_4{\cdot}3H_2O$ (see the Supporting Information

Received: February 1, 2015
Published: April 30, 2015

DOI: 10.1021/jacs.5b01100
J. Am. Chem. Soc. 2015, 137, 5859−5862

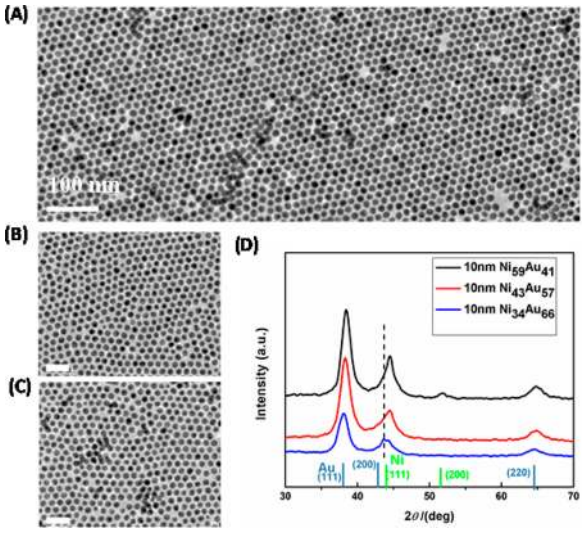

Figure 1. TEM images of the 10 nm $Ni_{43}Au_{57}$ (A), $Ni_{59}Au_{41}$ (B), $Ni_{34}Au_{66}$ (C) NPs (scale bar is 40 nm for B and C) and XRD patterns of the $Ni_{34}Au_{66}$, $Ni_{43}Au_{57}$ and $Ni_{59}Au_{41}$ NPs (D).

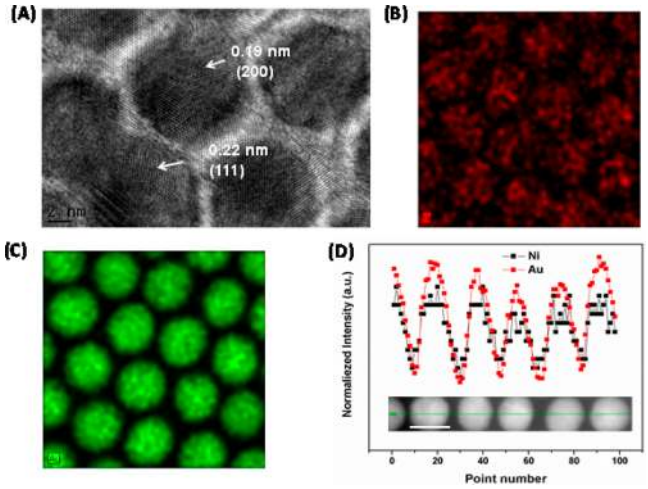

Figure 2. HRTEM image of the $Ni_{43}Au_{57}$ NPs (A), elemental mappings of Ni (red) (B), Au (green) (C) as well as line-scan EDS analysis across $Ni_{43}Au_{57}$ NPs (the inset shows the NPs scanned; scale bar = 10 nm) (D).

(SI)). The co-reduction method could be readily applied to synthesize CoAu and FeAu NPs (see the SI). Au and Ni NPs were also prepared as controls (see the SI).

Figure 1A–C shows representative transmission electron microscopy (TEM) images of the as-synthesized NiAu NPs with the different compositions. They are monodisperse with an average diameter of 10 ± 0.8 nm. CoAu, FeAu, and Au NPs can be controlled to be at the same size, but Ni NPs are only at 4 nm (Figure S1). The X-ray diffraction (XRD) patterns of the as-synthesized NiAu NPs show that the NPs have the face-centered cubic (fcc) structure (Figure 1D). The (111)/(200) peaks of the NiAu NPs locate between those of the Ni and Au NPs and shift to higher angels with the increase in Ni content in the NiAu NPs, indicating that Ni and Au form the fcc-structured solid solution.[11] We should note that the Ni-rich $Ni_{59}Au_{41}$ alloy NPs contain a small fraction of fcc-Ni phase as indicated by the presence of the weak fcc-Ni peaks. However, such contamination should not affect the catalytic observation due to the etching process applied in the catalyst preparation (see below for electrochemical cycling for catalyst preparation).

Figure 2A shows the high-resolution TEM (HRTEM) image of the as-prepared $Ni_{43}Au_{57}$ NPs. Two different lattice fringes are seen to have the spacing of 0.22 and 0.19 nm, corresponding to the (111) and (200) planes respectively on the NiAu alloy NP surface.[12] These lattice spacings are between those of Ni (111) (0.199 nm)/(200) (0.173 nm) and Au (111) (0.235 nm)/(200) (0.203 nm), which is consistent with the change of the lattice spacing observed from the XRD patterns and further proves the formation of the NiAu alloy structure.[13] The alloy formation was further characterized by elemental mapping and linear scan energy dispersive X-ray spectroscopy (EDS). Figure 2B–D shows a high-resolution elemental mapping of the 10 nm $Ni_{43}Au_{57}$ NPs and the EDS line scan across an array of the $Ni_{43}Au_{57}$ NPs, confirming that both Ni and Au distribute evenly in each NP.

To understand more about the NiAu alloy formation during the synthesis, we monitored the NP growth by TEM and sampled the reaction aliquots by ICP-AES. If no $Ni(acac)_2$ was added in the reaction, polydisperse Au NPs were obtained (Figure S2). If there was no $HAuCl_4 \cdot 3H_2O$ present, $Ni(acac)_2$ was reduced at about 200 °C, forming magnetic Ni NP precipitate. When $Ni(acac)_2$ and $HAuCl_4 \cdot 3H_2O$ were co-present, $Ni(acac)_2$ could be reduced at lower temperatures as reaction solution turned to darker color at only 80–120 °C, indicating the start of nucleation and growth of NiAu NPs. The ICP-AES analysis on the sample separated from the reaction solution heated at 150 °C for 30 min showed that the Ni/Au composition reached $Ni_{48}Au_{52}$. Reaction at higher temperature (220 °C) helped to incorporate more Au into the NiAu alloys, giving $Ni_{43}Au_{57}$. These synthetic studies showed that in the mixture of $HAuCl_4 \cdot 3H_2O$ and $Ni(acac)_2$, the reduction of $HAuCl_4 \cdot 3H_2O$ to Au initiates $Ni(acac)_2$ reduction at lower temperatures, forming NiAu alloys with the alloy compositions controlled by reaction temperatures; the higher the reaction temperature, the higher the Au content in the NiAu alloy NPs.

The HER catalyzed by the as-synthesized NiAu NPs was investigated in 0.5 M H_2SO_4 solution using a three-electrode setup with an Au wire as the counter electrode. A commercial C–Pt catalyst (2.5–3.5 nm Pt NPs in 20% mass loading, Fuel Cell Store) was used as a control. Figure 3A shows the HER polarization curves of different catalysts among which the C–$Ni_{43}Au_{57}$ exhibits the smallest onset potential (η) of ~70 mV. In contrast, the C–Ni or C–Au catalyst has much higher HER onset potential than the C–NiAu, which is consistent with what have been reported that pure Au and Ni NPs are less active catalysts for HER.[14]

The more dramatic aspect of these NiAu NPs is that their HER activity can be enhanced after continuous potential cycling from 0.6 to 1.0 V. Figure 3B highlights the HER results after the potential cycling on the C–$Ni_{43}Au_{57}$ catalyst. The HER onset potential shifts positively with the increased number of potential cycles, reaching the maximum and steady value after 20,000 cycles. The resultant catalyst shows the much reduced HER onset potential (~7 mV) that is close to that observed from the commercial C–Pt (Figure 3C). The catalytic activities of the C–$Co_{44}Au_{56}$ and C–$Fe_{47}Au_{53}$ NPs for the HER were also studied, as shown in Figure S3. After the same number of potential cycling treatments, both C–$Co_{44}Au_{56}$ and C–$Fe_{47}Au_{53}$ NPs become more active, showing the HER onset potentials that are similar to the value from the C–$Ni_{43}Au_{57}$ NPs.

The catalyst obtained after 20,000 potential cycles was analyzed by the elemental mapping and linear scan EDS. Figure

DOI: 10.1021/jacs.5b01100
J. Am. Chem. Soc. 2015, 137, 5859–5862

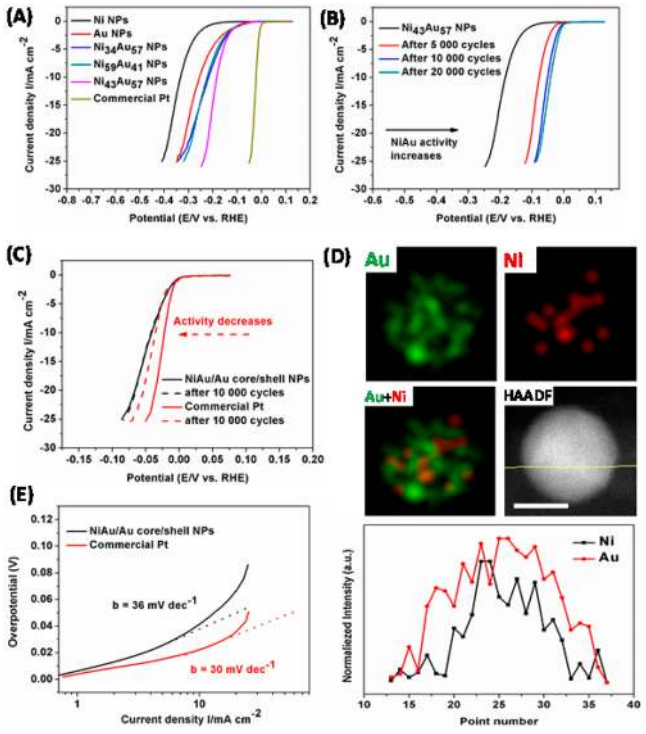

Figure 3. HER polarization curves of various as-prepared NP catalysts (A), the HER polarization curves of C−$Ni_{43}Au_{57}$ before and after cycling tests (B), the HER polarization curves of the NiAu/Au core/shell NPs and the commercial Pt before and after 10 000 cycling tests (C), elemental mapping and line-scan EDS analysis across a representative NiAu/Au core/shell NP (high-angle annular dark field shows the NPs scanned, scale bar = 5 nm) (D), Tafel plots recorded on the corresponding catalysts in 0.5 M H_2SO_4 solution (E).

3D shows the elemental mapping and EDS line scan on Ni/Au distribution within the $Ni_{43}Au_{57}$ NP after the cycling test. We can see that Au still spreads across the whole NP, but Ni is concentrated only in the center region of the NP, indicating that after potential cycling, the surface Ni in the NiAu NPs is etched away and the core/shell NiAu/Au is formed. The Ni etching from the NiAu structure was further confirmed by the ICP-AES analysis on the Ni/Au composition change from $Ni_{43}Au_{57}$ to $Ni_{24}Au_{76}$ after 20,000 potential cycling.

The core/shell NiAu/Au NPs are not only active but also durable for the HER. Their (as well as the commercial Pt) durability toward the HER was assessed by applying 10,000 potential sweeps between −0.3 and 0.9 V. Such sweeps caused substantial activity degradation for the Pt catalyst, but nearly no activity change for the NiAu/Au catalyst (Figure 3C), indicating that the core/shell NiAu/Au has much superior durability to Pt in catalyzing the HER in 0.5 M H_2SO_4.

On a catalyst surface, the HER process can be described by a Volmer−Heyrovsky mechanism ($H_3O^+ + e^- = H_{ads} + H_2O$ and $H_{ads} + H_3O^+ + e^- = H_2 + H_2O$) and/or a Tafel mechanism ($H_{ads} + H_{ads} = H_2$).[15] These two mechanisms infer that adsorption and desorption of H atoms on the catalyst surface are competitive and must be balanced to facilitate HER. The Tafel equation ($\eta = b \log j + a$, where j is the current density and b is the Tafel slope) is often used to study the rate-limiting step of the HER.[15a,b] A HER following the Volmer−Heyrovsky mechanism can have a significant overpotential and a large Tafel slope. The Tafel slope of C−$Ni_{43}Au_{57}$ is calculated to be about 43 mV dec^{-1} and is much smaller than either that of C−Ni (~75 mV dec^{-1}) or C−Au

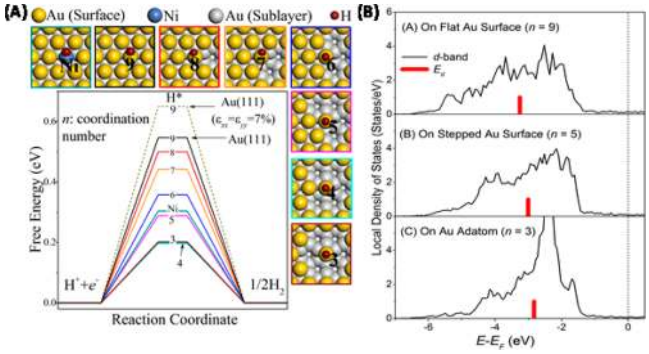

Figure 4. Free energy diagram for HER (U = 0 V) at Au sites with different coordination numbers n. Each line is labeled as the corresponding n. The broken line indicates G_{H^*} on 7%-strained Au (111). The line labeled as "Ni" indicates G_{H^*} at first NN of an isolated Ni site on Au (111). (A) LDOS on Au atom with (A) n = 9, (B) n = 5 and (C) n = 3. The red thick bar indicates the center of d-band, E_d, on the Au atom. The vertical broken line indicates the Fermi energy, E_F. (B).

(~78 mV dec^{-1}) (Figure S4). As a comparison, the Tafel slope of the NiAu/Au is about 36 mV dec^{-1}, similar to that of the commercial Pt catalyst (~30 mV dec^{-1}) (Figure 3E). These suggest that the recombination of two adsorbed H atoms is the rate-limiting step at low overpotentials.[15a,d] The study indicates that the formation of NiAu/Au pushes the HER to follow the Tafel mechanism.

To gain insight into the enhanced HER activity on NiAu and NiAu/Au NPs, we performed first-principles calculations using Vienna ab initio simulation package.[16] The central physical quantity of interest is free energy diagram from which one can assess the HER catalytic activity (see SI for computational details). We have calculated the free energy of hydrogen adsorption, G_{H^*}, on the Au (111) surface following the work of Nørskov et al.[17] As shown in the experiments, Ni atoms are removed continuously from the surface during the electrochemical cycling, we thus expect that structural defects, in particular vacancies would be formed on the alloy surface. As a result, the Au atoms adjacent to the defects would have lower coordination numbers n as compared to the perfect surface. It has been shown recently that on the Au (111) surface, an adsorption site with a lower n would exhibit a higher HER activity.[7c] We therefore hypothesize that the Au atoms adjacent to the defects can contribute to the enhanced HER activities. To confirm this hypothesis, we calculate G_{H^*} as a function of n on the Au (111) surface. More specifically, an H atom is adsorbed next to a Au atom, and G_{H^*} is calculated at zero bias potential as the neighboring Au atoms are removed one by one to create under-coordinated H adsorption sites. Seven defects with n ranging from 3 to 9 have been considered here. As depicted in Figure 4A, n = 3 represents an isolated Au adatom onto which the H is adsorbed; n = 8 and 9 corresponds to an adsorption site adjacent to a single vacancy and the perfect lattice, respectively. As shown in Figure 4A, G_{H^*} decreases monotonously with decreasing n, suggesting that the HER activity is enhanced as n becomes smaller. Therefore, the enhanced HER activity during the electrochemical cycling indeed results from the formation of under-coordinated Au sites. Furthermore, we have also considered a high-index (854) surface, containing flat terraces (n = 9), steps (n = 7), and kinks (n = 6 or 8), which are typical surface defects (Figure S5). For the same n value, we find that G_{H^*} at the (854) surface is very close to that on the (111) surface with vacancies. In other words, the under-coordinated Au atoms are

DOI: 10.1021/jacs.5b01100
J. Am. Chem. Soc. 2015, 137, 5859−5862

responsible for the enhanced HER activities independent of defect types. The results can be explained by the well-known *d*-band model that correlates the *d*-band center E_d, with adsorption energy.[18] We calculated local density of states (LDOS) projected onto three representative Au sites: the Au atom on the flat (111) surface ($n = 9$), the Au atom attaching to a step ($n = 5$), and an isolated Au adatom ($n = 3$). As shown in Figure 4B, as n decreases from 9 to 5 and 3, the *d*-band center shifts toward the Fermi energy, corresponding to stronger binding energy of H and thus a decrease of G_{H^*}. We also estimated the lattice mismatch between Au shell and $Ni_{50}Au_{50}$ core and found that NiAu core imposes a compressive strain (7%) on the Au shell. The strain increases G_{H^*} by 0.1 eV, which would lead to lower HER activities. Thus, the surface strain is not the origin of the enhanced HER activities during the cycling. Furthermore, the electronic effect of Ni in NiAu core to the Au shell catalysis is also minimal as FeAu/Au and CoAu/Au obtained after the same cycling treatment are nearly as active as NiAu/Au. Finally, we calculated G_{H^*} by placing a H atom adjacent to a Ni atom which substitutes for a Au atom as shown in Figures 4A and S5A. The calculated G_{H^*} is 0.25 eV lower than that on the pure surface, explaining the enhanced HER activity on NiAu alloy relative to the pure Au surface.

In summary, we have reported a facile synthesis of monodisperse NiAu NPs by co-reduction of $Ni(acac)_2$ and $HAuCl_4 \cdot 3H_2O$ at 220 °C. The NiAu NPs are more active catalyst for HER than either Ni or Au NPs. After electro-anodization, the NiAu alloy NPs are converted to core/shell NiAu/Au NPs, and their HER activity is increased significantly. The core/shell NiAu/Au has the Pt-like activity and is even more stable than the Pt in the HER condition, becoming the most efficient non-Pt catalyst ever reported for HER in acidic media. The first-principles calculations suggest that the high activity of core/shell structure arises from the formation of the Au sites with low coordination numbers. Analyses on the Tafel slopes reveal that the defected Au shell in the NiAu/Au structure facilitates the recombination of two adsorbed H atoms and therefore the HER. Our study provides a general approach to MAu alloy and MAu/Au core/shell NPs for catalytic tuning and optimization. The optimized MAu/Au can replace Pt to catalyze HER for important energy applications.

■ ASSOCIATED CONTENT

Supporting Information

Experiments, Computational methods, Figures S1-5, and Tables S1-2. The Supporting Information is available free of charge on the ACS Publications website at DOI: 10.1021/jacs.5b01100.

■ AUTHOR INFORMATION

Corresponding Authors

*ganglu@csun.edu
*msc@whut.edu.cn
*ssun@brown.edu

Author Contributions

‖These authors contributed equally.

Notes

The authors declare no competing financial interest.

■ ACKNOWLEDGMENTS

This work was supported by the U.S. Army Research Laboratory and the U.S. Army Research Office under the Multi University Research Initiative (MURI, grant no. W911NF-11-1-0353) on "Stress-Controlled Catalysis via Engineered Nanostructures" and by the China Scholarship Council (H.L.).

■ REFERENCES

(1) (a) Turner, J. A. *Science* **2004**, *305*, 972−974. (b) Dresselhaus, M. S.; Thomas, I. L. *Nature* **2001**, *414*, 332−337.

(2) (a) Mazloomi, K.; Gomes, C. *Renewable Sustainable Energy Rev.* **2012**, *16*, 3024−3033. (b) Nørskov, J. K.; Christensen, C. H. *Science* **2006**, *312*, 1322−1323.

(3) (a) McKone, J. R.; Warren, E. L.; Bierman, M. J.; Boettcher, S. W.; Brunschwig, B. S.; Lewis, N. S.; Gray, H. B. *Energy Environ. Sci.* **2011**, *4*, 3573−3583. (b) Popczun, E. J.; McKone, J. R.; Read, C. G.; Biacchi, A. J.; Wiltrout, A. M.; Lewis, N. S.; Schaak, R. E. *J. Am. Chem. Soc.* **2013**, *135*, 9267−9270.

(4) (a) Zheng, Y.; Jiao, Y.; Zhu, Y. L.; Li, L. H.; Han, Y.; Chen, Y.; Du, A. J.; Jaroniec, M.; Qiao, S. Z. *Nat. Commun.* **2014**, *5*, 4783 DOI: 10.1038/ncomms4783. (b) Cobo, S.; Heidkamp, J.; Jacques, P. A.; Fize, J.; Fourmond, V.; Guetaz, L.; Jousselme, B.; Ivanova, V.; Dau, H.; Palacin, S.; Fontecave, M.; Artero, V. *Nat. Mater.* **2012**, *11*, 802−807.

(5) (a) Green, L. X. Y.; Tang, W. J.; Neurock, M.; Yates, J. T., Jr. *Science* **2011**, *333*, 736−739. (b) Kimm, H. Y.; Lee, H. M.; Henkelman, G. *J. Am. Chem. Soc.* **2012**, *134*, 1560−1570.

(6) Lee, Y. M.; Loew, A.; Sun, S. H. *Chem. Mater.* **2012**, *22*, 755−761.

(7) (a) Kauffman, D. R.; Alfonso, D.; Matranga, C.; Qian, H. F.; Jin, R. C. *J. Am. Chem. Soc.* **2012**, *134*, 10237−10243. (b) Chen, Y. H.; Li, C. W.; Kanan, M. W. *J. Am. Chem. Soc.* **2012**, *134*, 19969−19972. (c) Zhu, W. L.; Michalsky, R.; Metin, Ö.; Lv, H. F.; Guo, S. J.; Wright, C. J.; Sun, X. L.; Peterson, A. A.; Sun, S. H. *J. Am. Chem. Soc.* **2013**, *135*, 16833−16836.

(8) (a) Zhang, S.; Zhang, X.; Jiang, G. M.; Zhu, H. Y.; Guo, S. J.; Su, D.; Lu, G.; Sun, S. H. *J. Am. Chem. Soc.* **2014**, *136*, 7734−7739. (b) Sun, X. L.; Li, D. G.; Ding, Y.; Zhu, W. L.; Guo, S. J.; Wang, Z. L.; Sun, S. H. *J. Am. Chem. Soc.* **2014**, *136*, 5745−5749.

(9) (a) Zhou, S. H.; Yin, H. F.; Schwartz, V.; Wu, Z. L.; Mullins, D.; Eichhorn, B.; Overbury, S. H.; Dai, S. *ChemPhysChem* **2008**, *9*, 2475−2479. (b) Zhou, S. H.; Ma, Z.; Yin, H.; Wu, Z.; Eichhorn, B.; Overbury, S.; Dai, S. *J. Phys. Chem. C* **2009**, *113*, 5758−5765.

(10) Yu, Y. S.; Yang, W. W.; Sun, X. L.; Zhu, W. L.; Li, X. Z.; Sellmyer, D. J.; Sun, S. H. *Nano Lett.* **2014**, *14*, 2778−2782.

(11) (a) Wang, D. L.; Xin, H. L.; Hovden, R.; Wang, H. S.; Yu, Y. C.; Muller, D. A.; Disalvo, F. J.; Abruña, H. D. *Nat. Mater.* **2012**, *12*, 81−87. (b) Cui, C. H.; Gan, L.; Heggen, M.; Rudi, S.; Strasser, P. *Nat. Mater.* **2013**, *12*, 765−771.

(12) Gong, K. P.; Su, D.; Adzic, R. R. *J. Am. Chem. Soc.* **2010**, *132*, 14364−14366.

(13) (a) Molenbroek, A. M.; Nørskov, J. K. *J. Phys. Chem. B* **2001**, *105*, 5450−5458. (b) Chen, W.; Yu, R.; Li, L. L.; Wang, A. N.; Peng, Q.; Li, Y. D. *Angew. Chem.* **2010**, *122*, 2979−2983.

(14) (a) Perez, J.; Gonzalez, E. R. *J. Phys. Chem. B* **1998**, *102*, 10931−10935. (b) Hinnemann, B.; Moses, P. G.; Bonde, J.; Jørgensen, K. P.; Nielsen, J. H.; Horch, S.; Chorkendorff, I.; Nørskov, J. K. *J. Am. Chem. Soc.* **2005**, *127*, 5308−5309.

(15) (a) Li, Y. G.; Wang, H. L.; Xie, L. M.; Liang, Y. Y.; Hong, G. S.; Dai, H. J. *J. Am. Chem. Soc.* **2011**, *133*, 7296−7299. (b) Chen, W. F.; Sasali, K.; Ma, C.; Frenkel, A. I.; Marinkovic, N.; Muckerman, J. T.; Zhu, Y. M.; Adizc, R. R. *Angew. Chem., Int. Ed.* **2012**, *51*, 6131−6135. (c) Huang, X.; Zeng, Z. Y.; Bao, S. Y.; Wang, M. F.; Qi, X. Y.; Fan, Z. X.; Zhang, H. *Nat. Commun.* **2014**, *4*, 1444 DOI: 10.1038/ncomms2472. (d) Markovic, N. M.; Grgur, B. N.; Ross, P. N. *J. Phys. Chem. B* **1997**, *101*, 5405−5413.

(16) (a) Kresse, G.; Hafner, J. *Phys. Rev. B* **1993**, *47*, 558−561(R). (b) Kresse, G.; Furthmüller, J. *Phys. Rev. B* **1996**, *54*, 11169−11186.

(17) Nørskov, J. K.; Bligaard, T.; Logadottir, A.; Kitchin, J. R.; Chen, J. G.; Pandelov, S.; Stimming, U. *J. Electrochem. Soc.* **2005**, *152*, J23−J26.

(18) (a) Mavrikakis, M.; Hammer, B.; Nørskov, J. K. *Phys. Rev. Lett.* **1998**, *81*, 2819−2822. (b) Hammer, B.; Nørskov, J. K. *Nature* **1995**, *376*, 238−240.

DOI: 10.1021/jacs.5b01100
J. Am. Chem. Soc. 2015, 137, 5859−5862